

# Coherent control of Snell's law at metasurfaces

Jinhui Shi,<sup>1,2\*</sup> Xu Fang,<sup>2</sup> Edward T. F. Rogers,<sup>2,3</sup> Eric Plum,<sup>2</sup> Kevin F. MacDonald,<sup>2</sup> and Nikolay I. Zheludev<sup>2,4</sup>

<sup>1</sup> Key Laboratory of In-Fiber Integrated Optics of Ministry of Education, College of Science, Harbin Engineering University, Harbin 150001, China

<sup>2</sup> Optoelectronics Research Centre and Centre for Photonic Metamaterials, University of Southampton, SO17 1BJ, UK

<sup>3</sup> Institute for Life Sciences, University of Southampton, SO17 1BJ, UK

<sup>4</sup> Centre for Disruptive Photonic Technologies, Nanyang Technological University, Singapore 637378, Singapore  
\*hrbeusjh@gmail.com

**Abstract:** It was recently demonstrated that the well-known Snell's law must be corrected for phase gradient metasurfaces to account for their spatially varying phase, leading to normal and anomalous transmission and reflection of light on such metasurfaces. Here we show that the efficiency of normal and anomalous transmission and reflection of light can be controlled by the intensity or phase of a second coherent wave. The phenomenon is illustrated using gradient metasurfaces based on V-shaped and rectangular apertures in a metal film. This coherent control effect can be exploited for wave front shaping and signal routing.

©2014 Optical Society of America

**OCIS codes:** (160.3918) Metamaterials; (260.2110) Electromagnetic optics; (310.6628) Subwavelength structures, nanostructures.

---

## References and links

1. A. Papakostas, A. Potts, D. M. Bagnall, S. L. Prosvirnin, H. J. Coles, and N. I. Zheludev, "Optical Manifestations of Planar Chirality," *Phys. Rev. Lett.* **90**(10), 107404 (2003).
2. N. Yu, P. Genevet, M. A. Kats, F. Aieta, J. P. Tetienne, F. Capasso, and Z. Gaburro, "Light propagation with phase discontinuities: generalized laws of reflection and refraction," *Science* **334**(6054), 333–337 (2011).
3. X. Ni, N. K. Emani, A. V. Kildishev, A. Boltasseva, and V. M. Shalaev, "Broadband light bending with plasmonic nanoantennas," *Science* **335**(6067), 427 (2012).
4. S. Sun, K. Y. Yang, C. M. Wang, T. K. Juan, W. T. Chen, C. Y. Liao, Q. He, S. Y. Xiao, W. T. Kung, G. Y. Guo, L. Zhou, and D. P. Tsai, "High-efficiency broadband anomalous reflection by gradient meta-surfaces," *Nano Lett.* **12**(12), 6223–6229 (2012).
5. T. Roy, A. E. Nikolaenko, and E. T. F. Rogers, "A meta-diffraction-grating for visible light," *J. Opt.* **15**(8), 085101 (2013).
6. M. Kang, T. Feng, H.-T. Wang, and J. Li, "Wave front engineering from an array of thin aperture antennas," *Opt. Express* **20**(14), 15882–15890 (2012).
7. Z. Y. Wei, Y. Cao, X. P. Su, Z. J. Gong, Y. Long, and H. Q. Li, "Highly efficient beam steering with a transparent metasurface," *Opt. Express* **21**(9), 10739–10745 (2013).
8. X. B. Yin, Z. L. Ye, J. Rho, Y. Wang, and X. Zhang, "Photonic spin Hall effect at metasurfaces," *Science* **339**(6126), 1405–1407 (2013).
9. G. X. Li, M. Kang, S. M. Chen, S. Zhang, E. Y. B. Pun, K. W. Cheah, and J. Li, "Spin-enabled plasmonic metasurfaces for manipulating orbital angular momentum of light," *Nano Lett.* **13**(9), 4148–4151 (2013).
10. P. Genevet, N. Yu, F. Aieta, J. Lin, M. A. Kats, R. Blanchard, M. O. Scully, Z. Gaburro, and F. Capasso, "Ultra-thin plasmonic optical vortex plate based on phase discontinuities," *Appl. Phys. Lett.* **100**(1), 013101 (2012).
11. N. Yu, F. Aieta, P. Genevet, M. A. Kats, Z. Gaburro, and F. Capasso, "A broadband, background-free quarter-wave plate based on plasmonic metasurfaces," *Nano Lett.* **12**(12), 6328–6333 (2012).
12. S. Sun, Q. He, S. Xiao, Q. Xu, X. Li, and L. Zhou, "Gradient-index meta-surfaces as a bridge linking propagating waves and surface waves," *Nat. Mater.* **11**(5), 426–431 (2012).
13. X. Chen, L. Huang, H. Mühlenbernd, G. X. Li, B. Bai, Q. Tan, G. Jin, C. W. Qiu, S. Zhang, and T. Zentgraf, "Dual-polarity plasmonic metalens for visible light," *Nature Commun* **3**, 1198 (2012).
14. X. Ni, S. Ishii, A. V. Kildishev, and V. M. Shalaev, "Ultra-thin, planar, Babinet-inverted plasmonic metalenses," *Light Sci. Appl.* **2**(4), e72 (2013).
15. A. Pors, M. G. Nielsen, R. L. Eriksen, and S. I. Bozhevolnyi, "Broadband focusing flat mirrors based on plasmonic gradient metasurfaces," *Nano Lett.* **13**(2), 829–834 (2013).

16. G. Yuan, E. T. F. Rogers, T. Roy, Z. Shen, and N. I. Zheludev, "Flat super-oscillatory lens for heat-assisted magnetic recording with sub-50 nm resolution," *Opt. Express* **22**(6), 6428–6437 (2014).
17. J. Lin, P. Genevet, M. A. Kats, N. Antoniou, and F. Capasso, "Nanostructured holograms for broadband manipulation of vector beams," *Nano Lett.* **13**(9), 4269–4274 (2013).
18. X. Ni, A. V. Kildishev, and V. M. Shalaev, "Metasurface holograms for visible light," *Nature Comm.* **4**, 2807 (2013).
19. L. L. Huang, X. Chen, H. Muhlenbernd, H. Zhang, S. Chen, B. Bai, Q. Tan, G. Jin, K.-W. Cheah, C.-W. Qiu, J. Li, T. Zentgraf, and S. Zhang, "Three-dimensional optical holography using a plasmonic metasurface," *Nature Comm.* **4**, 2808 (2013).
20. W. T. Chen, K.-Y. Yang, C.-M. Wang, Y.-W. Huang, G. Sun, I.-D. Chiang, C. Y. Liao, W.-L. Hsu, H. T. Lin, S. Sun, L. Zhou, A. Q. Liu, and D. P. Tsai, "High-efficiency broadband meta-hologram with polarization-controlled dual images," *Nano Lett.* **14**(1), 225–230 (2014).
21. J. Zhang, K. F. MacDonald, and N. I. Zheludev, "Controlling light-with-light without nonlinearity," *Light: Sci. Appl.* **1**(7), e18 (2012).
22. X. Fang, M. L. Tseng, D. P. Tsai, and N. I. Zheludev, "Coherent excitation-selective spectroscopy in planar metamaterials," <http://arxiv.org/abs/1312.0524> (2013).
23. X. Fang, M. L. Tseng, J. Y. Ou, K. F. MacDonald, D. P. Tsai, and N. I. Zheludev, "Ultrafast all-optical switching via coherent modulation of metamaterial absorption," *Appl. Phys. Lett.* **104**(14), 141102 (2014).
24. J. F. Zhang, C. C. Guo, K. Liu, Z. H. Zhu, W. M. Ye, X. D. Yuan, and S. Q. Qin, "Coherent perfect absorption and transparency in a nanostructured graphene film," *Opt. Express* **22**(10), 12524–12532 (2014).
25. S. A. Mousavi, E. Plum, J. H. Shi, and N. I. Zheludev, "Coherent control of birefringence and optical activity," *Appl. Phys. Lett.* **105**(1), 011906 (2014).
26. COMSOL 3.5a.
27. Z. T. Liu, A. Boltasseva, R. H. Pedersen, R. Bakker, A. V. Kildishev, V. P. Drachev, and V. M. Shalaev, "Plasmonic nanoantenna arrays for the visible," *Metamaterials (Amst.)* **2**(1), 45–51 (2008).

## 1. Introduction

When light is incident on a metasurface with a gradient phase change along the surface, reflection and refraction follow a generalized form of Snell's law and the phase change imposed by interaction with meta-molecules allows anomalous reflection and refraction [1–5]. Recently, substantial efforts have been devoted to the exploration of gradient metasurfaces, leading to the demonstration of wave-front shaping [6,7], the photonic spin Hall effect [8,9], an optical vortex plate [10], broadband optical retardation [11], a propagating-to-surface-wave converter [12], flat lenses and mirrors [13–15], super-oscillatory focusing [16] and optical holograms [17–20]. It was also recently shown that absorption [21–24], and polarization effects due to anisotropy and chirality [25], in a thin metasurface can be controlled by a second wave incident on the same surface. In this paper we demonstrate that reflection and refraction effects on phase gradient metasurfaces can be coherently controlled by a second wave.

We investigate two gradient metasurfaces constructed from an array of either V-shaped apertures or rectangular slits in a freestanding gold film of substantially subwavelength thickness. The V-shaped metasurface produces a cross-polarized anomalous transmitted beam while the slit metasurface produces a co-polarized one. Both normal and anomalous outgoing beams can be coherently controlled for both metasurface designs. The gradient metasurfaces are ultrathin freestanding gold nanostructures with varying geometries within a super cell, which can be practically fabricated from a gold-coated  $\text{Si}_3\text{N}_4$  membrane using focused-ion-beam milling and reactive ion etching.

## 2. V-shaped antenna metasurface

Our first candidate metasurface for coherent control is the commonly used V-shaped antenna metasurface [2, 3, 8, 10, 11, 14, 17, 18]. This metasurface supports both anomalous and normal reflected/transmitted beams and the anomalous reflected and refracted beams possess linear polarization perpendicular to both the incident excitation and the normal beams allowing for easy discrimination [2]. The unit cell comprises eight V-shaped slot antennas with a periodicity of  $d_x$  in the  $x$  direction and  $d_y$  in the  $y$  direction. The structure is cut from an ultrathin gold film with a thickness of  $t = 50\text{nm}$  (Fig. 1(a)), generating a gradient phase shift

$d\phi$  along the  $x$  direction. The structural details of the V-shaped slot antennas are shown in the inset of Fig. 1(a). Here,  $d_x = 8d = 1600\text{nm}$  and  $d_y = d = 200\text{nm}$ . The slot arms have variable lengths  $l$  and a fixed width  $w = 40\text{nm}$ . The V-shaped slot antennas have variable azimuthal angles  $\beta$  and opening angles  $\gamma$ . The parameters of each antenna in the super cell are shown in Table 1.

**Table 1. Parameters of the V-shaped antennas in each super cell**

	1	2	3	4	5	6	7	8
$\beta$ ( $^\circ$ )	45	45	45	45	-45	-45	-45	-45
$\gamma$ ( $^\circ$ )	60	90	120	180	60	90	120	180
$l$ (nm)	158	145	110	93	158	145	110	93

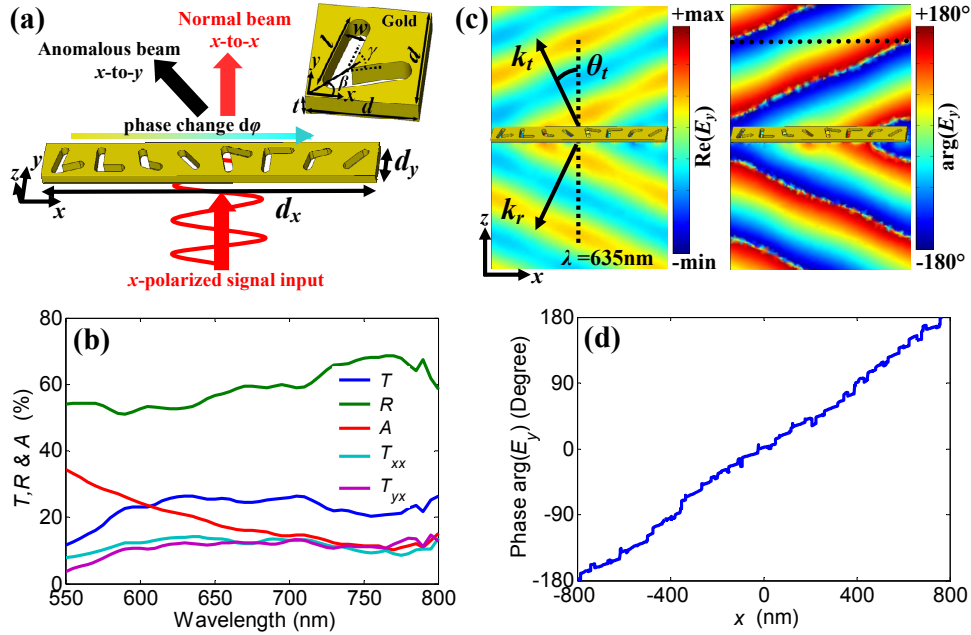


Fig. 1. Schematic and simulated optical properties of the V-shaped slot metasurface for a single input beam. (a) Schematic of the anomalous and normal transmitted beams for an  $x$ -polarized incident beam propagating in the  $z$  direction. The inset shows the structural details of the V-shaped slot antennas. (b) The simulated total intensity of transmission  $T$ , reflection  $R$  and absorption  $A$ ; and the polarization selected intensities of the anomalous  $T_{yx}$  and normal  $T_{xx}$  transmitted beams. (c) Amplitude and phase maps of the scattered field  $E_y$  for a wavelength of  $635\text{nm}$ . Arrows indicate the propagation directions of anomalous refracted and reflected beams. (d) Lineout of phase across one super cell along the dotted line in panel c. The eight slot nanoantennas radiate  $y$ -polarized light with phases from  $-180^\circ$  to  $180^\circ$ . Noise is seen in this curve due to interpolation across the finite sized mesh elements.

For an  $x$ -polarized single beam normally incident along the  $z$  direction, this gradient metasurface has co-polarized normal transmitted/reflected beams and cross-polarized anomalous refracted/reflected beams. The normal  $x$ -polarized beams propagate along the  $z$  direction, as expected. The directions of anomalous  $y$ -polarized refracted and reflected beams are governed by the generalized Snell's law as follows [2],

$$\begin{aligned}
 n_t \sin(\theta_t) - n_i \sin(\theta_i) &= \frac{\lambda}{2\pi} \frac{d\varphi}{dx} \\
 \sin(\theta_r) - \sin(\theta_i) &= \frac{\lambda}{2\pi n_i} \frac{d\varphi}{dx}
 \end{aligned}
 \tag{1}$$

Where  $\theta_i$ ,  $\theta_t$  and  $\theta_r$  are the angles of incidence, transmission and reflection respectively and  $\lambda$  is the wavelength. Here we assume that transmission and reflection are into free space, so the refractive indices are  $n_t = n_i = 1$ . Based on full-wave simulations using a full three-dimensional Maxwell finite element method solver [26], the total transmitted, reflected and absorbed intensities are shown in Fig. 1(b), where the permittivity of gold was described by the Drude-Lorentz model [27]. The total transmission (reflection) includes the output intensities of both the anomalous and normal transmitted (reflected) beams. The V-shaped slot metasurface exhibits broadband anomalous refraction as well as anomalous reflection. The anomalous refracted and transmitted beams are emitted by the metasurface and as a scattering interface of essentially zero thickness radiates the same scattered field in the forward and backward directions, both anomalous beams have the same intensity and angle of refraction and reflection. While our discussion mainly focuses on transmitted beams, our findings on anomalous refraction will equally apply to anomalous reflection. At a wavelength of 635 nm, the output intensities  $T_{yx}$  and  $T_{xx}$  of the anomalous and normal transmitted beams are about 12% and 14% while the absorption is about 20%. The scattered  $E_y$  field amplitude and phase maps of the gradient metasurface at 635 nm are shown in Fig. 1(c). The eight slot antennas radiate  $y$ -polarized light with almost constant amplitude and phases  $\varphi$  gradually changing from  $-180^\circ$  to  $+180^\circ$  across the super cell (Fig. 1(d)) forming the anomalous beams. The anomalous beams approximate plane waves with propagation directions that are significantly different from the normal beams. Simulations show identical angles of refraction  $\theta_t$  and reflection  $\theta_r$  of about  $23^\circ$ , consistent with the theoretical calculation  $\theta_t = \theta_r = \sin^{-1}(635/1600) = 23.4^\circ$  according to Eq. (1).

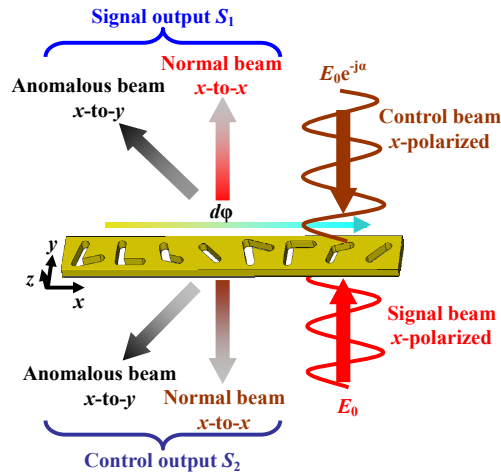


Fig. 2. Schematic of coherent control of the V-shaped slot antennas metasurface using coherent signal and control beams. Both input beams are  $x$ -polarized with a phase difference  $\alpha$ .

Next we investigate how this gradient metasurface response is affected by an additional control beam of the same polarization as, and coherent with, the incident signal beam (see Fig. 2). The two beams have a relative phase difference  $\alpha$ . The coherent counter-propagating beams form a standing wave interference pattern and the scattering from the metasurface is determined by the position of the surface in this standing wave. In the limiting cases, a

gradient metasurface of substantially subwavelength thickness can be placed either at an electric anti-node or node, leading to enhanced or vanishing electric excitation, and therefore scattering, respectively. Both signal and control output intensities  $S_1$  and  $S_2$  consist of contributions from the anomalous and normal output beams.  $S = S_1 + S_2$  is the total output intensity, while  $A = 2 - S$  is absorption. The input intensities of the signal and control beams are defined as 100% each and thus the total output intensity is 200% in the case of zero absorption. Figure 3(a) shows that the intensities of the output beams and the total absorption depend strongly on the phase difference between the control and signal beams. As the phase difference  $\alpha$  increases from  $0^\circ$  to  $180^\circ$ , absorption  $A$  in the 50nm-thick gradient metasurface decreases from 78% to 2.8% while the corresponding total output intensity  $S$  increases from 122% to 197.2%.

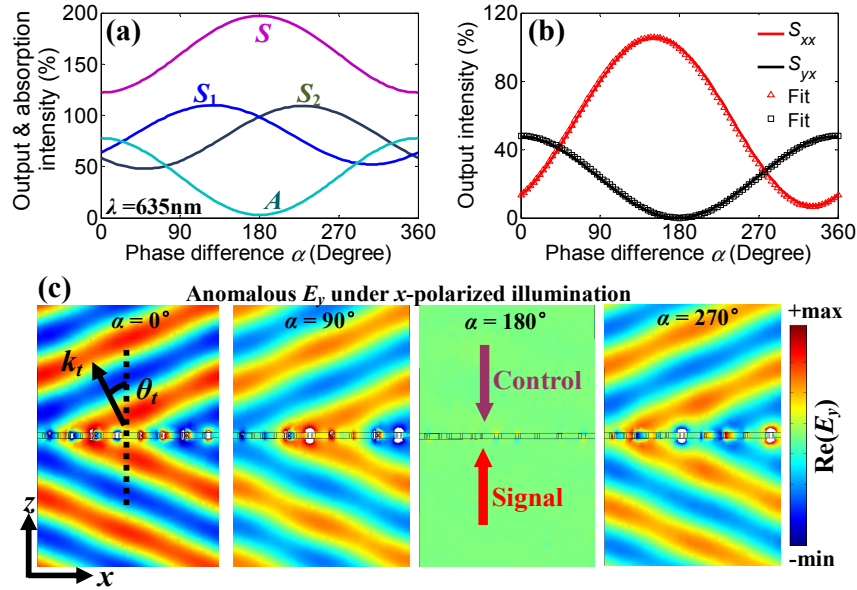


Fig. 3. Coherent control of the gradient metasurface of V-shaped slot antennas for a wavelength of 635nm. (a) Total output intensity  $S$  and absorption  $A$  of the gradient metasurface as a function of the phase difference  $\alpha$  between the  $x$ -polarized control and signal incident beams.  $S_1$  and  $S_2$  indicate the signal and control outputs, respectively. (b) Output intensities  $S_{yx}$  and  $S_{xx}$  of the anomalous and normal beams forming the signal output  $S_1$  as a function of  $\alpha$ . The triangle and square symbols indicate sinusoidal fits. (c) Simulated scattered  $E_y$  field magnitude maps for  $\alpha = 0^\circ, 90^\circ, 180^\circ$  and  $270^\circ$ . All color maps of the electric field are plotted on the same scale as Fig. 1(c).

The signal output intensity  $S_1$  is used to illustrate how the anomalous and normal beams are coherently controlled ( $S_1 = S_{yx} + S_{xx}$ ). In Fig. 3(b) we see that for in-phase excitation ( $\alpha = 0^\circ$ ) of the metasurface, this is when the metasurface is placed at an electric anti-node of the standing wave formed by the incident beams, the electric excitation field doubles, leading to an increase of the anomalous output beam intensity. In comparison to  $T_{yx} = 12\%$  for single beam excitation, the total anomalous beam output in the coherent control case increases fourfold to 48%. For anti-phase excitation ( $\alpha = 180^\circ$ ), this is when the metasurface is placed at an electric node of the standing wave and its interaction with the standing wave is negligible, the anomalous output beam intensity  $S_{yx}$  decreases to zero and the normal output beam intensity  $S_{xx}$  is nearly 100%. This near-perfect plasmonic transparency is achieved because the gradient metasurface is simply not excited when  $\alpha = 180^\circ$ . The anomalous and normal output beam intensities show a sinusoidal dependence on the phase difference  $\alpha$  shown in Fig. 3(b). In order to visualize the amplitude and propagation direction of the anomalous beams, Fig. 3(c) presents the simulated scattered  $E_y$  field patterns of the gradient

metasurface for  $\alpha = 0^\circ, 90^\circ, 180^\circ$  and  $270^\circ$ . All color maps of the electric fields are plotted on the same scale as Fig. 1(c). Both anomalous reflected and refracted beams vanish in the case of  $\alpha = 180^\circ$  when the gradient metasurface is located at an electric node of the standing wave. In contrast to the intensity, the propagation direction of the anomalous beams is insensitive to the phase difference  $\alpha$  between the control and signal beams and the refracted/reflected angles of the anomalous beams are always about  $23^\circ$ . This is because the coherent control process controls the overall level of scattering from the structure but does not change the phase gradient imposed by the metasurface, which is determined solely by the metasurface design. This allows simple modulation of the output beam intensities through phase control without distorting or redirecting the individual beams. Although we use a fixed wavelength of 635nm, this coherent control technique can be applied over a broad range of wavelengths [25] and promises many applications such as wave front shaping and signal routing.

### 3. Slot antenna metasurface

Next, we discuss another important gradient metasurface which generates an anomalous beam with the same polarization as the incident beam [4,15]. The negative metasurface is also cut from an ultrathin gold film with a thickness of  $t = 50\text{nm}$ . The unit cell comprises ten rectangular slot antennas with a periodicity of  $a_x$  in the  $x$  direction and  $a_y$  in the  $y$  direction (Fig. 4(a)), generating a gradient phase shift  $d\phi$  along the  $x$  direction. A schematic of a rectangular slot antenna is given in the inset of Fig. 4(a). Here,  $a_x = 10p_x = 1200\text{nm}$  and  $a_y = p_y = 300\text{nm}$ . The rectangular slits have variable lengths  $l$  and a fixed width  $w = 50\text{nm}$ .  $l = 40, 40, 106, 106, 128, 128, 150, 150, 260$  and  $260$  nm, respectively. This type of metasurface is known not to display polarization conversion [4]. For  $x$ -polarized single beam excitation along the  $z$  direction, this gradient metasurface has  $x$ -polarized normal and anomalous transmitted beams. The normal transmitted beam propagates along the  $z$  direction while the direction of the anomalous  $x$ -polarized refracted beam is governed by the generalized Snell's law.

The simulated total intensities of transmission, reflection and absorption are shown in Fig. 4(b). The total transmission includes the output intensities of the anomalous and normal transmitted beams. The rectangular slot metasurface exhibits broadband anomalous refraction as well as anomalous reflection. In contrast to the V-shaped antenna case, the normal and anomalous beams have the same polarization. Simulated amplitude and phase maps of the total transmitted field  $E_x$  at  $\lambda = 635$  nm for normally incident  $x$ -polarized excitation are shown in Fig. 4(c) and the corresponding lateral phase change of the transmitted field along the dotted line is shown in Fig. 4(d). Obviously the output field  $E_x$  is not a single plane wave, since the normally propagating beam and the deflected anomalous beam have the same polarization and so both contribute to the total transmitted field  $E_x$ . Generally, it is difficult to tell the anomalous beam from the electric field distribution.

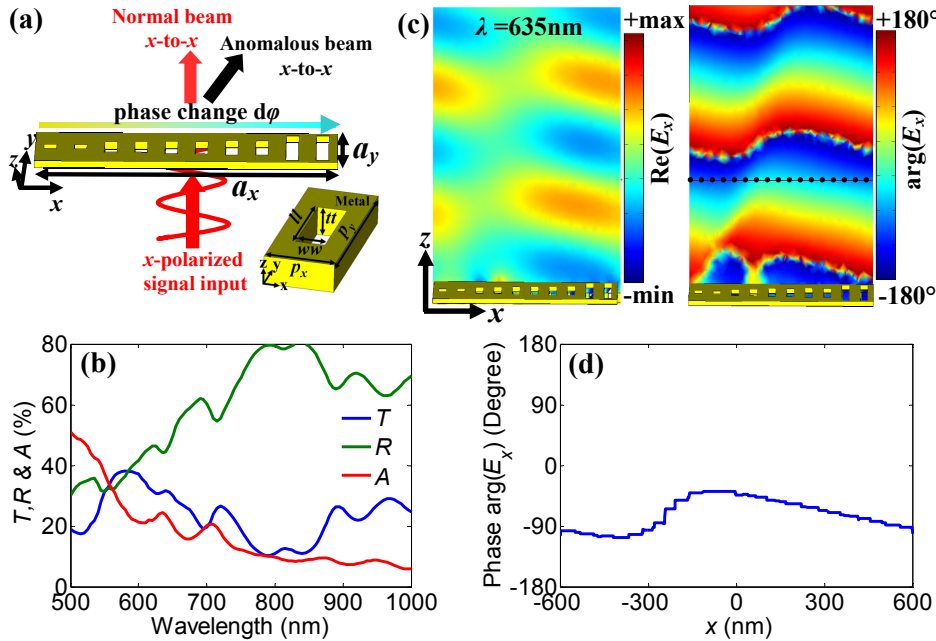


Fig. 4. Schematic and the simulated optical properties of the rectangular slot metasurface for a single input beam. (a) Schematic of the anomalous and normal transmitted beams for a single  $x$ -polarized input beam incident on the gradient metasurface along the  $z$  direction. The unit cell comprises ten rectangular slot antennas with a periodicity of  $a_x$  in the  $x$  direction and  $a_y$  in the  $y$  direction, generating a gradient phase shift along the  $x$  direction. The inset shows the structural details of the rectangular slot antennas. (b) Transmission  $T$ , reflection  $R$  and absorption  $A$  spectra. (c)  $E_x$  amplitude and phase maps of the transmitted field for a wavelength of 635nm showing the superposition of the  $x$ -polarized normal ( $T_{nor} = 23\%$ ) and anomalous ( $T_{ano} = 8.4\%$ ) beams. (d) Phase of the transmitted wave within a super cell along the dotted line in panel c.

We next examine how the gradient metasurface with rectangular slot antennas is affected by an additional coherent control beam of the same polarization as the incident signal beam (similar to the scheme in Fig. 2). When the phase difference  $\alpha$  between the control and signal beams varies, the standing wave pattern moves with respect to the gradient metasurface and we thus achieve enhanced or vanishing electric excitation of the rectangular slot antennas. Figure 5(a) shows that the intensity of the signal output beam, control output beam and absorption are efficiently modulated by the control beam, similar to the gradient metasurface with V-shaped slot antennas. The total absorption  $A$  of the rectangular slot metasurface decreases from 95.1% to 2.7% and the corresponding total output intensity increases from 104.9% to 197.3% as the phase difference  $\alpha$  increases from  $0^\circ$  to  $180^\circ$ . As above, the signal intensity  $S_1$  is used to investigate coherent control of the anomalous and normal beams ( $S_1 = S_{ano} + S_{nor}$ ), see Fig. 5(b). At a wavelength of  $\lambda = 635\text{nm}$  for single beam illumination, the intensities  $S_{ano}$  and  $S_{nor}$  are 8.4% and 23%, while the absorption is 24.5%. As expected, for in-phase electrical excitation ( $\alpha = 0^\circ$ ) of the metasurface, the total anomalous output beam intensity increases approximately fourfold compared with single beam excitation. On the other hand, for anti-phase excitation ( $\alpha = 180^\circ$ ), the anomalous output beam intensity  $S_{ano}$  decreases to zero and the normal output beam intensity  $S_{nor}$  is nearly 100%.

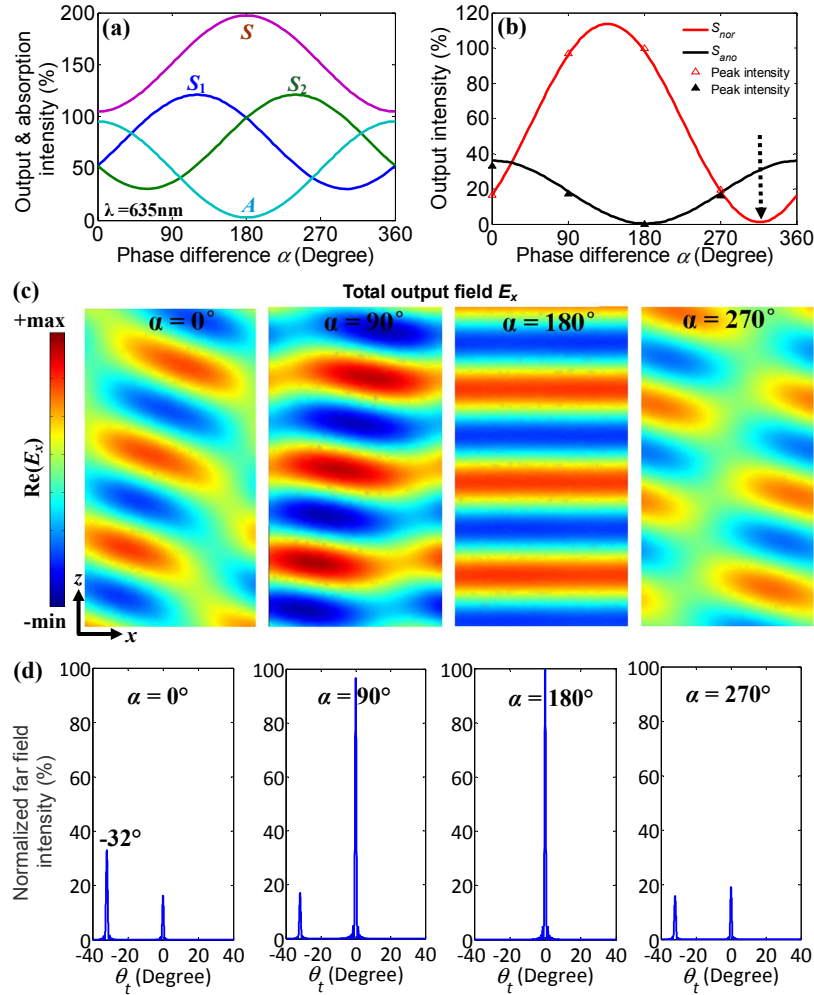


Fig. 5. Coherent control of the gradient metasurface of rectangular slot antennas for a wavelength of 635nm. (a) Total output  $S$ , signal output  $S_1$  and control output  $S_2$  intensities and absorption  $A$  of the gradient metasurface as a function of the phase difference  $\alpha$  between the control and signal beams. (b) Intensities  $S_{ano}$  and  $S_{nor}$  of the anomalous and normal beams comprising the signal output  $S_1$  as a function of  $\alpha$ .  $S_{nor}$  is nearly zero at  $\alpha = 320^\circ$  indicated by the arrow. The empty and solid triangles correspond to the normal and anomalous beam intensities in the far field calculations of panel d. (c)  $E_x$  field patterns of the signal output for  $\alpha = 0^\circ, 90^\circ, 180^\circ$  and  $270^\circ$ . All color maps are on the same scale. (d) Normalized far field intensity as a function of refraction angle  $\theta_t$  for the phase differences  $\alpha = 0^\circ, 90^\circ, 180^\circ$  and  $270^\circ$ .

Figure 5(c) presents the total signal output field patterns  $E_x$  of the gradient metasurface for  $\alpha = 0^\circ, 90^\circ, 180^\circ$  and  $270^\circ$ . It is clearly seen that the wave front of the output beam changes with the phase difference  $\alpha$  and the output is not a plane wave except for  $\alpha = 180^\circ$ . When  $\alpha = 180^\circ$ , the signal output beam is a perfect plane wave due to the vanishing anomalous beam, consistent with Fig. 5(b). However, we cannot easily characterize the direction of the anomalous beam from this metasurface since its polarization is identical to that of the normal beam. By taking the Fourier transform of the output electric field, we calculate the far field pattern and find the directions and intensities of the normal and anomalous beams as illustrated in Fig. 5(d), which has been normalized by the far field peak intensity of the signal beam in absence of the metasurface. The refraction angles of the

normal and anomalous beams are  $0^\circ$  and  $-32^\circ$ , respectively. The predicted peak values of the far field intensity of the anomalous and normal beams are in good agreement with the FEM simulations shown in Fig. 5(b). As seen above, when the phase difference  $\alpha$  varies, the output intensities of both the normal and anomalous beams are modulated, but the refraction angles remain unchanged. Therefore, this fundamental characteristic of preserving refracted directions is identical to the gradient metasurface with V-shaped slot antennas regardless of the phase gradient design and the polarization of the anomalous output beam. Interestingly, there is an alternative way to determine the propagation direction of the anomalous beam. Both the output intensities of the normal and anomalous beams have a sinusoidal dependence on the phase difference. At a phase difference of  $\alpha = 320^\circ$ , the normal beam intensity  $S_{nor}$  is suppressed to zero, here the normal beam contributions from the signal and control inputs cancel each other. Figure 6 presents amplitude and phase of the signal output field  $E_x$  for the gradient metasurface at  $\alpha = 320^\circ$ . In absence of the field of the normal beam, it can be clearly seen that the anomalous beam is approximately a plane wave with a refraction angle of  $-32^\circ$ , exactly consistent with the far field calculation in Fig. 5(d). This simulated result also agrees well with the theoretical prediction based on the generalized Snell's law,  $\theta_t = \sin^{-1}(-635/1200) = -31.95^\circ$ . Thus, coherent control can be used to select the anomalous beam from the total signal output.

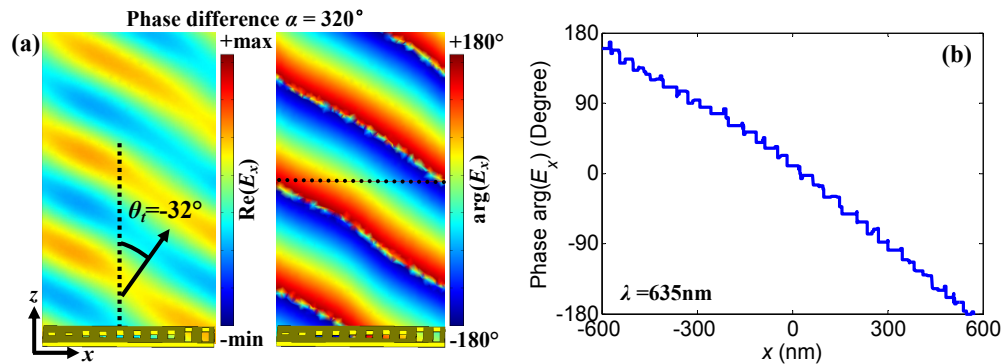


Fig. 6. (a)  $E_x$  field amplitude and phase maps of the signal output beam of the gradient rectangular slot metasurface for  $x$ -polarized coherent illumination with phase difference  $\alpha = 320^\circ$  and wavelength  $635\text{nm}$ . The arrow indicates the propagation direction of the anomalous refracted beam. (b) Phase of the signal output within a super cell along the dotted line in panel a. Here, the signal output field has a linear phase gradient from  $180^\circ$  to  $-180^\circ$  resulting in an anomalous output beam without simultaneous presence of the normal output beam.

#### 4. Conclusions

In summary, we have demonstrated that excitation of ultrathin metasurfaces can be controlled using the relative phase of two coherent input beams, for two phase gradient metasurfaces with very different scattering behaviours. We have shown for the first time, that normal and anomalous beams following the generalized Snell's law can be coherently controlled, strongly modulated and separately switched on/off by changing the phase difference between two counterpropagating coherent control and signal input beams. In the coherent control regime, the propagation directions of both the normal and anomalous output beams remain unaltered while the amount of energy in each output beam has a sinusoidal dependence on the phase difference between the input beams. In particular, coherent control can determine how energy is distributed between normal and anomalous output beams with the same or opposite polarizations. Coherently controlled metasurfaces promise many new applications including signal routing, wavefront shaping and scattered field manipulation.

## **Acknowledgments**

This work is supported by the MOE Singapore (grant MOE2011-T3-1-005), the Leverhulme Trust, the Royal Society and the UK's Engineering and Physical Sciences Research Council through the Nanostructured Photonic Metamaterials Programme (Grant EP/G060363/1). J.S. acknowledges support from the National Science Foundation of China under grant No. 61201083 and the 111 Project under Grant No. B13015. ETFR acknowledges support from the University of Southampton Enterprise Fund.